Hindawi Publishing Corporation
Advances in Meteorology
Volume 2014, Article ID 592106, 12 pages
http://dx.doi.org/10.1155/2014/592106

Research Article

Forest Phenology Dynamics and Its Responses to Meteorological Variations in Northeast China

Xinfang Yu,[1] Qiankun Wang,[1,2] Huimin Yan,[1] Yong Wang,[1] Kege Wen,[1] Dafang Zhuang,[1] and Qiao Wang[3]

[1] *State Key Lab of Resources and Environmental Information System, Institute of Geographic Science and Natural Resources Research, Chinese Academy of Sciences, Beijing 100101, China*
[2] *Southwest Forestry University, Kunming 650000, China*
[3] *State Environmental Protection Key Laboratory of Satellite Remote Sensing, Satellite Environment Center, Ministry of Environmental Protection of People's Republic of China, Beijing 100094, China*

Correspondence should be addressed to Xinfang Yu; yuxf@igsnrr.ac.cn

Received 14 February 2014; Revised 30 April 2014; Accepted 15 May 2014; Published 4 June 2014

Academic Editor: Shengli Huang

Based on time series of Moderate Resolution Imaging Spectroradiometer (MODIS) Enhanced Vegetation Index (EVI) data (2000–2009), we extracted forest phenological variables in Northeast China using a threshold-based method, which included the start of the growing season (SOS), end of the growing season (EOS), and length of the growing season (LOS). The spatial variation of phenological trends was analyzed using the linear regression method. In Northeast China, SOS was delayed at the rate of <1.5 days per year. The delay trend of EOS was well distributed in the entire region with almost the same rates. LOS increased slightly. The analysis of the relationship between forest phenology and meteorological variations shows that SOS was mainly affected by spring temperature, whereas SOS had a negative relationship with precipitation in the warm-temperate deciduous broadleaf forest region. The EOS in temperate steppe region was affected by temperature and precipitation in August, whereas the others were significantly affected by temperature. Because of the increased temperature in spring, the LOS of the temperate steppe region and temperate mixed forest region increased, and the LOS was positively correlated with the mean temperature of summer in the cool-temperate needleleaf forest region.

1. Introduction

Phenology has proven to be a sensitive and integrative indicator of climate variability and vegetation growth responses to climate change [1, 2]. The understanding of phenology brings significant insight into both climate and vegetation interactions and their impacts on different spatial and temporal scales [3]. There is growing evidence that the ecological equilibrium has been altered due to global climate change, resulting in changes in vegetation cover over time and in space. Phenology monitoring can serve as an efficient way to understand the interactions between vegetation and climate, and repeated observations from satellite sensors provide the mechanism to move from plant-specific to regional scale studies of phenology. Satellite-derived vegetation indices are commonly used as indicators of vegetation phenology [4–10]. Justice et al. [4] used Normalized Difference Vegetation Index (NDVI) to qualitatively assess the global phenology of numerous land cover types. Satellites were later used to interpret phenology as an indicator of land cover changes in South America [5] and to detect phenological dynamics in shrublands [6]. White et al. [7] integrated the basic concepts of traditional meteorologically based phenology modeling with intensive satellite phenology observations and produced biome-specific ecosystem phenology models. Duchemin et al. [8] developed a method that consists of a fit of NDVI predicted by line segment to advanced very high resolution radiometer (AVHRR) NDVI time series to monitor two key stages, budburst and senescence, in the phenological cycle of deciduous forests. Zhang et al. [9, 10] used a series of piecewise logistic functions fit to MODIS Vegetation Index (VI) data to monitor four key transition phases of vegetation dynamics at annual temporal scales. Much related research has demonstrated that environmental drivers such as climate,

topography, and soil properties affect vegetation dynamics at different spatial and temporal scales, ranging from instant to long-term and from local to regional scales [11–18].

Some literatures have described Chinese vegetation phenology research using remotely sensed data. Chen et al. studied the relationship between plant phenology and satellite sensor derived measures of greenness in Eastern China based on field phenological data and NOAA AVHRR data [19–23]. Zhang et al. found that green-up dates in the Tibetan Plateau have continuously advanced from 1982 to 2011 [24]. Guo et al. analyzed Global Inventory Modeling and Mapping Studies (GIMMS) NDVI time series between 1982 and 2003 and found that the start of the growing season of vegetation in Northeast China was significantly influenced by spring temperature [25]. Mao et al. demonstrated that precipitation was a major factor in determining the characteristics of phenology in permafrost regions [26]. Most of these previous studies were limited by spatial resolution (from 1 km to 8 km) and temporal resolution. Since the launch of Terra satellite in late 1999, its MODIS sensor on board provided daily coverage with 250 m spatial resolution.

The objective of this study is to analyze the spatial pattern of key forest phenological variables and to explore the relationship between phenology and meteorological variables in Northeast China. In this study, the 500 m, 8-day composite product from the Terra satellite of Earth Observing System was used to calculate Enhanced Vegetation Index (EVI) for 2000–2009. Spatial distribution maps of vegetation phenological variables were established based on 10-year EVI data, and phenological variables were then analyzed at the regional scale. The relationships between phenology and meteorological variables were analyzed after coupling with meteorological data.

2. Data and Methodology

2.1. Study Area. The study area is in Northeast China (115°09′–135°52′E and 38°72′–53°55′N), including Jilin, Heilongjiang, and Liaoning Provinces and eastern Inner Mongolia (Figure 1). The climates in Northeast China are warm-temperate, temperate, and cool-temperate. According to the vegetation regionalization map of 2001, Northeast China is categorized into four vegetation zones, that is, a cool-temperate needleleaf forest region, temperate needleleaf and broadleaf mixed-forest region, warm-temperate deciduous broadleaf forest region, and temperate steppe region (Figure 2) (Editorial Board of Vegetation Map of China, 2001). Northeast China has abundant tree species and a variety of forest types [27]. The forests are widely distributed over mountainous terrain (e.g., Daxinganling and Xiaoxinganling Ranges) and show large variation in species composition across latitudinal domains, elevation gradients, and moisture gradients. At low elevations, the dominant tree species include Korean pine (*Pinus koraiensis*), basswood (*Tilia amurensis*), oak (*Quercus mongolica*), painted maple (*Acer mono*), and ash (*Fraxinus mandshurica*). At high elevations, the major tree species include spruce (*Picea jezoensis* var. *microsperma*), fir (*Abies nephrolepis*), Mongolia pine (*Pinus*

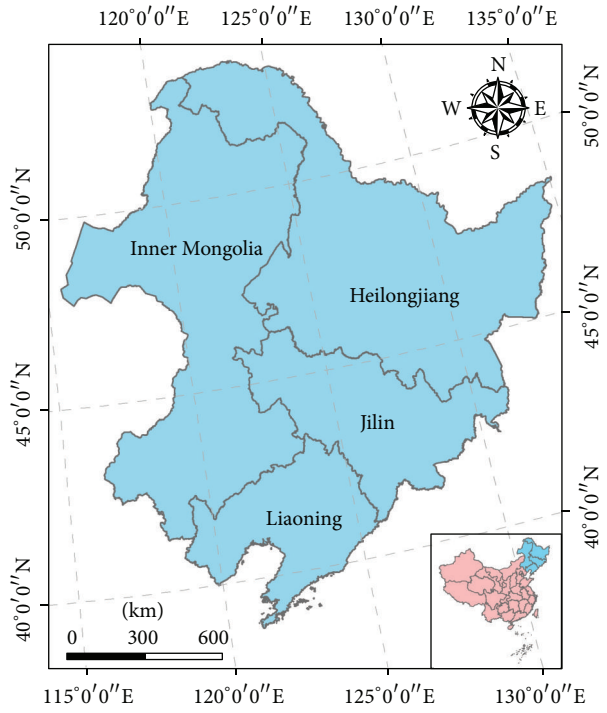

Figure 1: Province boundaries in Northeast China.

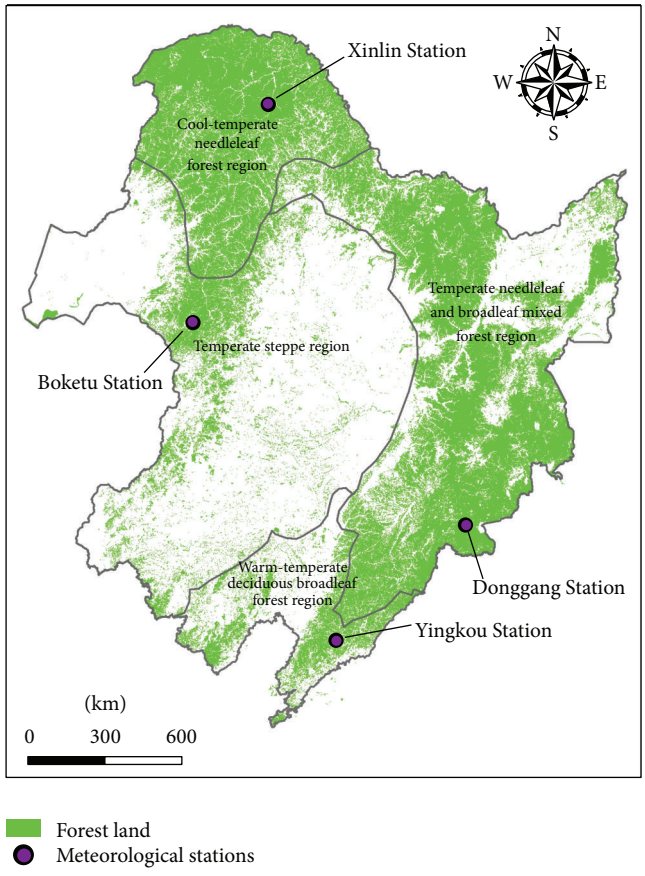

Figure 2: Vegetation zones in Northeast China.

sylvestris var. *mongolica*), aspen (*Populus davidiana*), and birch (*Betula platyphylla*). Deciduous coniferous larch (*Larix gmelinii*) forests are widely distributed in the most northern part of Northeast China.

2.2. Materials

2.2.1. MODIS EVI Data. The MODIS Land Science Team provides 8-day composite products for users. The 8-day Land Surface Reflectance product (MOD09A1) from 2000 to 2009 was used in this study. The data were downloaded from the EROS Data Center, US Geological Survey (https://lpdaac.usgs.gov/products/modis_products_table/mod09a1). The MOD09A1 product contains seven spectral bands with a spatial resolution of 500 m. The Enhanced Vegetation Index (EVI) was calculated using three-band reflectance data.

EVI directly adjusts the reflectance in the red band as a function of the reflectance in the blue band, accounting for residual atmospheric contamination (e.g., aerosols), variable soil, and canopy background reflectance [28]. EVI is linearly correlated with the leaf area index and has a higher sensitivity than that of NDVI in areas of high biomass [29]. The equation for EVI is as follows:

$$\mathrm{EVI} = 2.5 \times \left(\frac{p_{\mathrm{nir}} - p_{\mathrm{red}}}{L + p_{\mathrm{nir}} + C_1 p_{\mathrm{red}} - C_2 p_{\mathrm{blue}}} \right), \quad (1)$$

where $C_1 = 6$, $C_2 = 7.5$, and $L = 1$; p_{nir}, p_{red}, and p_{blue} are the reflectance of the blue, red, and near infrared bands, respectively.

2.2.2. Land Use Data. To study forest phenology individually, the forest zones of Northeast China were extracted from the entire region based on the 1 : 100,000 Land Use Map of China of 2000 from the Data Center for Resources and Environment Sciences, Chinese Academy of Sciences [30].

2.2.3. Climate Data. Air temperature data and rainfall data were acquired from the Chinese Meteorological Data Sharing Service System (http://cdc.cma.gov.cn/), including daily average air temperature and precipitation at 343 meteorological stations within the study area from 2000 to 2009. In this study, four representative stations located in Northeast China were used: Xinlin Station (N51.7°, E124.33°) in the cool-temperate needleleaf forest region, Boketu Station (N48.77°, E121.93°) in the temperate steppe region, Donggang Station (N42.1°, E127.57°) in the Temperate needleleaf and broadleaf mixed-forest region, and Yingkou Station (N40.65°, E122.17°) in the warm-temperate deciduous broadleaf forest region.

2.3. Methods. As shown in Figure 3, the double logistic fitting method was used to reduce noise in the time series MODIS EVI data. The threshold-based method was then used to extract forest phenological variables. The least square method was used to analyze the trend of 10 years of phenological variables. Lastly, the change trend was linked to the meteorological variables.

2.3.1. Double Logistic Fitting Method. The double logistic (D_L) function [31, 32] can be used as a basis function as follows:

$$g(t; a_1, \ldots, a_4) = \frac{1}{1 + \exp\left((a_1 - t)/a_2\right)} - \frac{1}{1 + \exp\left((a_3 - t)/a_4\right)}, \quad (2)$$

where a_1 and a_2 determine the position of the left and right inflection points of the curve, respectively, and a_2 and a_4 determine the rate of change at the left and right inflection points, respectively. The TIMESAT software [33] was used to fit the asymmetric Gaussians (AG), D_L, and Savizky-Glolay (SG) models. The AG and D_L functions are superior to the SG with regard to noise reduction [34]. The D_L model was used to fit the time series data in this study. After the data preprocessing of the Double Logistic fitting, the output data had litter noise, and the coefficients of fitted logistic functions were saved for each pixel.

2.3.2. Forest Phenological Variables. Considering the regional characteristics of the forests in Northeast China and the basic rationale of the above methods, the threshold-based method was used to identify forest phenology.

EVI percentage thresholds of 0.2 and 0.27 were used to justify the start of the growing season (SOS) and the end of the growing season (EOS), respectively, according to previous studies [35–37]. For a series of EVI in a given year, we detected $\mathrm{EVI}_{\mathrm{max}}$ as the maximum EVI and $\mathrm{EVI}_{\mathrm{min}}$ as the minimum EVI in the first half of the year. The SOS EVI value for a given pixel was calculated using the formula

$$\mathrm{EVI}_{\mathrm{start}} = \mathrm{EVI}_{\mathrm{min}} + \left(\mathrm{EVI}_{\mathrm{max}} - \mathrm{EVI}_{\mathrm{min}}\right) \times 0.2. \quad (3)$$

Then, the day of $\mathrm{EVI}_{\mathrm{start}}$ was determined as the SOS. The EOS was defined using the same method as follows:

$$\mathrm{EVI}_{\mathrm{end}} = \mathrm{EVI}_{\mathrm{min}} + \left(\mathrm{EVI}_{\mathrm{max}} - \mathrm{EVI}_{\mathrm{min}}\right) \times 0.27, \quad (4)$$

where $\mathrm{EVI}_{\mathrm{min}}$ is the minimum EVI in the last half of the year.

The processing was performed pixel by pixel to determine $\mathrm{EVI}_{\mathrm{start}}$ and $\mathrm{EVI}_{\mathrm{end}}$. SOS and EOS were then determined using the double logistic fitting results, which can be determined for a specific day with the above EVI thresholds. By using the percentage thresholds, the absolute EVI value could be adapted to each pixel, which makes the phenology more reasonable.

2.3.3. Trend Analysis and Its Linkage to Meteorological Variations. The linear regression method was used to analyze the trends of phenological variables. The least square method is a commonly used method in the analysis of vegetation growth [38] as follows:

$$L = \frac{n \times \sum_{j=1}^{n} j \times T_j - \sum_{j=1}^{n} j \sum_{j=1}^{n} T_j}{n \times \sum_{j=1}^{n} j^2 - \left(\sum_{j=1}^{n} j\right)^2}, \quad (5)$$

where n is the number of the years, T_j is the SOS of the j-year, and L is the slope of the trend line. If $L > 0$, the SOS

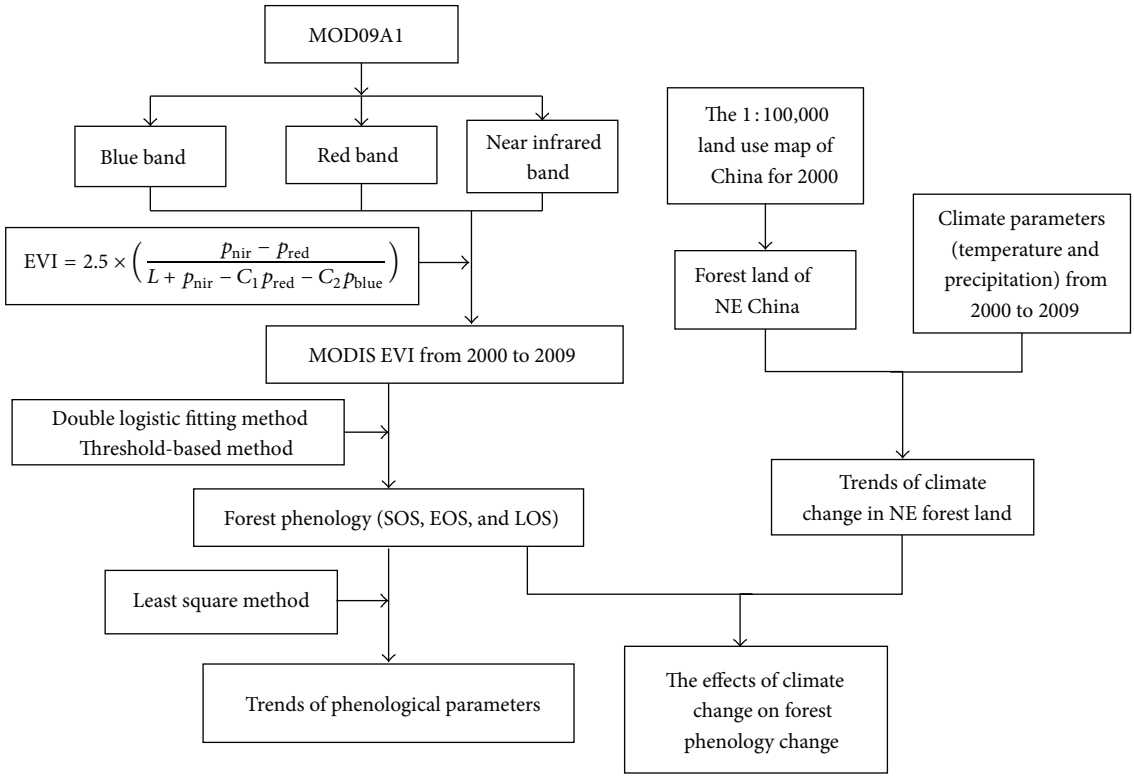

Figure 3: Flowchart and schematic of the study analysis.

had a delaying trend during 2000–2009; otherwise, the SOS had an advancing trend. SPSS 16.0 was used for the regression analysis for each pixel.

The interannual variations of phenology variables might be associated with the interannual variations of meteorological variables at regional scales. The connection between the changes in forest phenology (SOS, EOS, and LOS) and meteorological variations was analyzed. The effects of climate change on forest phenology trends were analyzed based on the phenological changes in the four major forest regions.

3. Results

3.1. Spatial Pattern of Forest Phenology. The 10-year annual EVI was calculated for each pixel, and the spatial pattern of forest phenology was generated based on the above-defined thresholds. The spatial distribution of the 10-year average phenological variables (SOS, EOS, and LOS) for Northeast China from 2000 to 2009 is shown in Figure 4. Table 1 shows the maximum, minimum, and average values of the phenological variables in the study area.

Figure 4(a) shows the SOS in Northeast China during DOY (day of the year) 100–140. SOS began earlier in the south, and greening occurred gradually toward the north. This is consistent with the period of tree leaf unfolding in spring. Figure 4(b) shows that the EOS ranges from the DOY 265 to 300, with the end of growth arriving later in lower latitudes, which corresponds to the period of defoliation in autumn. In the cool-temperate needleleaf forest region, there were some patches with an earlier SOS and later EOS, which were related to the evergreen needleleaf species of Mongolian pine. In general, the LOS mainly ranged from DOY 130 to 200 along latitudes from north to south in Northeast China, as shown in Figure 4(c).

Table 1: Range of phenological variables in SOE, EOS, and LOS in Northeast China.

Phenology	Maximum	Minimum	Mean
SOS	155	81	114
EOS	343	246	278
LOS	312	108	164

The spatial patterns of forest phenology in this study are consistent with previous research results [35, 39] and published field-observed phenological data [19–21]. Yu et al. used the threshold-based method to determine the SOS and EOS of Northeast China and found the SOS from DOY 100 to 150, the EOS from DOY 260 to 290, and the LOS mainly from 140–180 DOY [35]. Guo et al. found a DOY of 118–135 for SOS and 252–263 for EOS in Northeast China [39]. Comparison between these results showed that the results derived from the three phenological variables are reasonable in the present study.

3.2. Spatial Change of Phenology Trends. The spatial distribution of trends in the variables SOS and EOS for Northeast China over 10 years from 2000 to 2009 is provided in Figure 5. To evaluate annual trends in the phenological variables, these variables were analyzed at the vegetation zone scale.

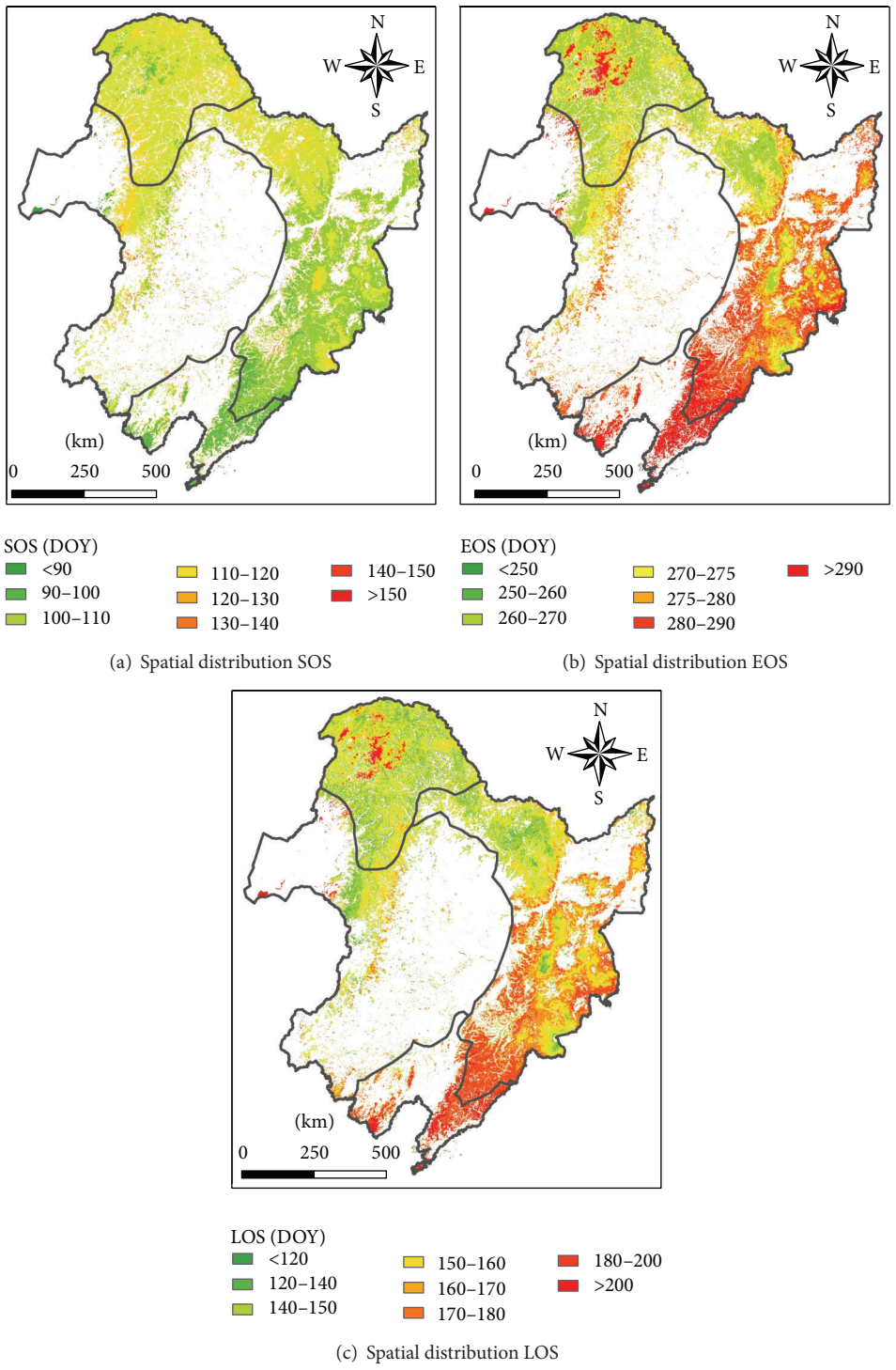

(a) Spatial distribution SOS

(b) Spatial distribution EOS

(c) Spatial distribution LOS

Figure 4: Spatial pattern of 10-year average forest phenology in Northeast China using MODIS EVI data of 2000~2009.

Figure 5(a) shows that the SOS was delayed with rates of 0~1.5 days per year for most pixels in the region. Although both advanced and delayed EOS were observed in the vegetation regionalization, the delay trend was more pervasive, with almost the same rates (Figure 5(b)). As a result, the LOS increased slightly (Figure 5(c)).

Table 2 demonstrates the linear trends of the area-averaged phenological variables (SOS, EOS, and LOS) in different vegetation zones of Northeast China. The average SOS advanced by 0.06 days per year in the warm-temperate deciduous broadleaf forest region, whereas SOS was delayed in the other three vegetation zones. The average EOS was

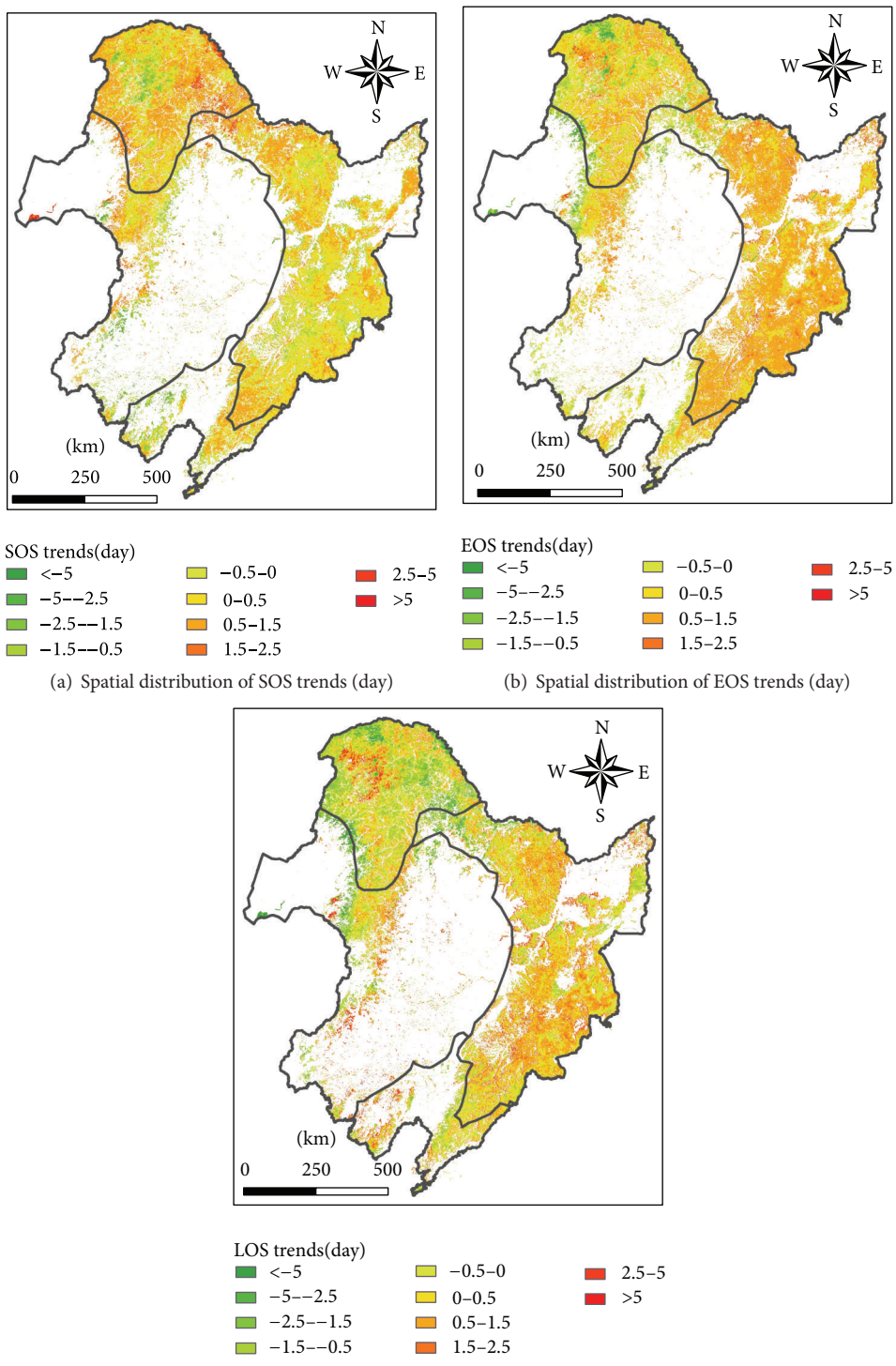

(a) Spatial distribution of SOS trends (day)

(b) Spatial distribution of EOS trends (day)

(c) Spatial distribution of LOS trends (day)

FIGURE 5: Spatial pattern of 10-year forest phenology change trends in Northeast China using MODIS EVI data of 2000~2009.

delayed in all of the vegetation zones. The increased delay in SOS in the cool-temperate needleleaf forest zone caused a decreased LOS (Table 2). The average LOS of the other vegetation zones was increased, and the most positive trend was approximately 0.58 days per year in the warm-temperate deciduous broadleaf forest zone.

3.3. *Effects of Climate Change on Forest Phenology Trends*

3.3.1. Climate Change. According to the meteorological data, we built the significant trends in meteorological parameters (mean temperature and mean precipitation) for Northeast China over 10 years from 2000 to 2009 (Table 3).

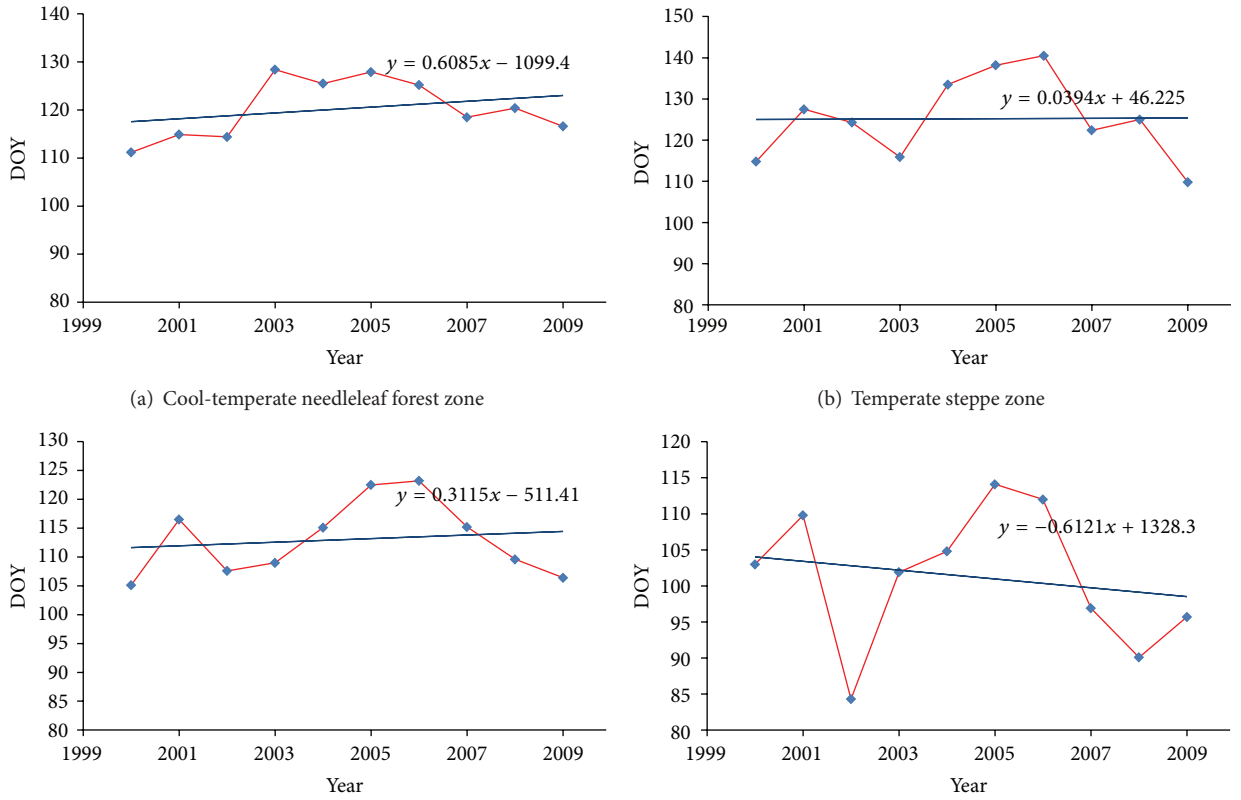

Figure 6: The average SOS trends in four forest zones.

Table 2: Linear trends of area-averaged phenological variables (SOS, EOS, and LOS) in different vegetation zones of Northeast China.

Regions	SOS trends		EOS trends		LOS trends	
	Slope (d·a^{-1})	Variance	Slope (d·a^{-1})	Variance	Slope (d·a^{-1})	Variance
I	0.50	1.27	0.27	1.54	−0.08	3.08
II	0.24	3.54	0.35	2.47	0.57	5.87
III	0.27	1.17	0.75	0.8	0.58	2.17
IV	−0.06	1.86	0.266	0.66	0.39	2.83

Note. I: cool-temperate needleleaf forest region; II: temperate steppe region; III: temperate needleleaf and broadleaf mixed forest region; IV: warm-temperate deciduous broadleaf forest region.

Table 3: Meteorological parameters (temperature and precipitation) in different vegetation zones of Northeast China.

Regions	Temperature (°C)		Precipitation (mm)	
	Mean (°C)	Slope (°C·a^{-1})	Mean (mm)	Slope (mm·a^{-1})
I	−2.05	0.04	1.42	0.03
II	0.22	0.07	1.11	0.04
III	4.19	0.05	2.18	0.02
IV	10.14	0.05	1.55	−0.03

Note. I: cool-temperate needleleaf forest region; II: temperate steppe region; III: temperate needleleaf and broadleaf mixed forest region; IV: warm-temperate deciduous broadleaf forest region.

The positive linear trend of temperature in the entire study area showed increasing temperature. The largest increase in temperature was observed in the temperate steppe region, at 0.07°C per year. The precipitation in the warm-temperate deciduous broadleaf forest region decreased at the rate of 0.03 mm per year. The average precipitation in the other three vegetation zones increased by the average rate of 0.03 mm per year.

3.3.2. Phenology Trends near Meteorological Stations. Using a window of 20 × 20 pixels centered at the selected meteorological stations, we calculated the average phenology metrics for each area. Figures 6, 7, and 8 show the trends of the average forest phenology for each meteorological station. These trends near the meteorological stations were consistent with each vegetation region.

3.3.3. Correlation Analysis between Phenology and Meteorological Variations. To analyze the effects of climate change

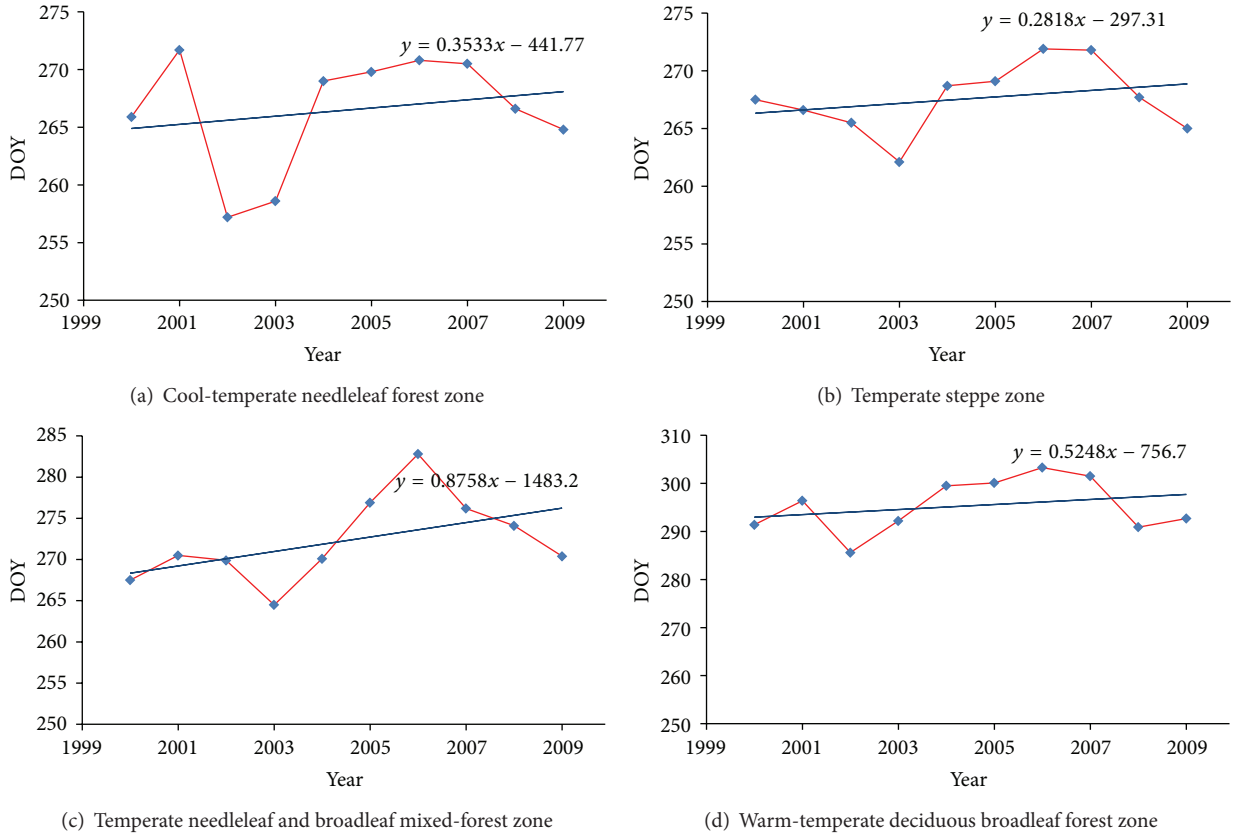

Figure 7: The average EOS trends in four vegetation zones.

on forest phenology trends, a correlation analysis between meteorological variations and phenology was used.

During 2000–2009, a series of temporal windows of February, March, April, May, spring (from March to May), the winter of the previous year (from December to the next February), and the entire previous year were used to calculate the mean meteorological variables (temperature and precipitation). These meteorological statistics were used as independent variables because they can represent the regional climate environment when SOS occurred in the study area.

Table 4 shows the correlation between meteorological variations and SOS (Table 4). The SOS of the cool-temperate needleleaf forest region had a relatively high negative relationship with the mean temperature of May ($R = -0.72$, $P < 0.01$). In the temperate steppe region, SOS had a negative relationship with the mean spring temperature ($R = -0.7$, $P < 0.05$), especially with the mean temperature of April ($R = -0.73$, $P < 0.01$). For the total needleleaf forest and temperate steppe region, no significant correlation was found between SOS and mean precipitation in all seasons. Thus, the SOS of the cool-temperate needleleaf forest and temperate steppe region was strongly affected by temperature. The SOS of the temperate needleleaf and broadleaf mixed-forest region showed a negative relationship correlation with the mean temperature of spring ($R = -0.69$, $P < 0.05$) and March ($R = -0.58$, $P < 0.05$), whereas it was positively correlated with the mean precipitation of the previous year ($R = 0.66$, $P < 0.05$). In addition, in the warm-temperate deciduous broadleaf forest region, SOS had a strongly negative relationship with the mean temperature of March ($R = -0.8$, $P < 0.01$), and the mean precipitation of March had a negative relationship with the SOS ($R = -0.55$, $P < 0.05$). The SOS of the cool-temperate needleleaf forest and temperate steppe region was separately affected by the mean temperature of May and April.

Similar to the SOS correlation analysis, a series of temporal windows of July–November, summer (from June to August), and autumn (from September to November) were used to calculate the mean meteorological variables (temperature and precipitation) for the EOS correlation analysis. Table 5 shows that the EOS of the cool-temperate needleleaf forest region was significantly positively correlated with the mean temperature of autumn ($R = 0.71$, $P < 0.01$) and the mean temperature of November ($R = 0.68$, $P < 0.05$). In the temperate needleleaf and broadleaf mixed-forest region, the EOS was positively correlated with the mean temperature of October ($R = 0.54$, $P < 0.05$), and the EOS of the deciduous broadleaf forest region had a strongly positive correlation with the mean temperature of autumn ($R = 0.79$, $P < 0.01$). For the above-mentioned three regions, EOS was weakly correlated with the mean precipitation in all seasons. Table 5 shows that EOS was affected by temperature more strongly than precipitation. The temperature and precipitation of August both affected the EOS in the temperate steppe region.

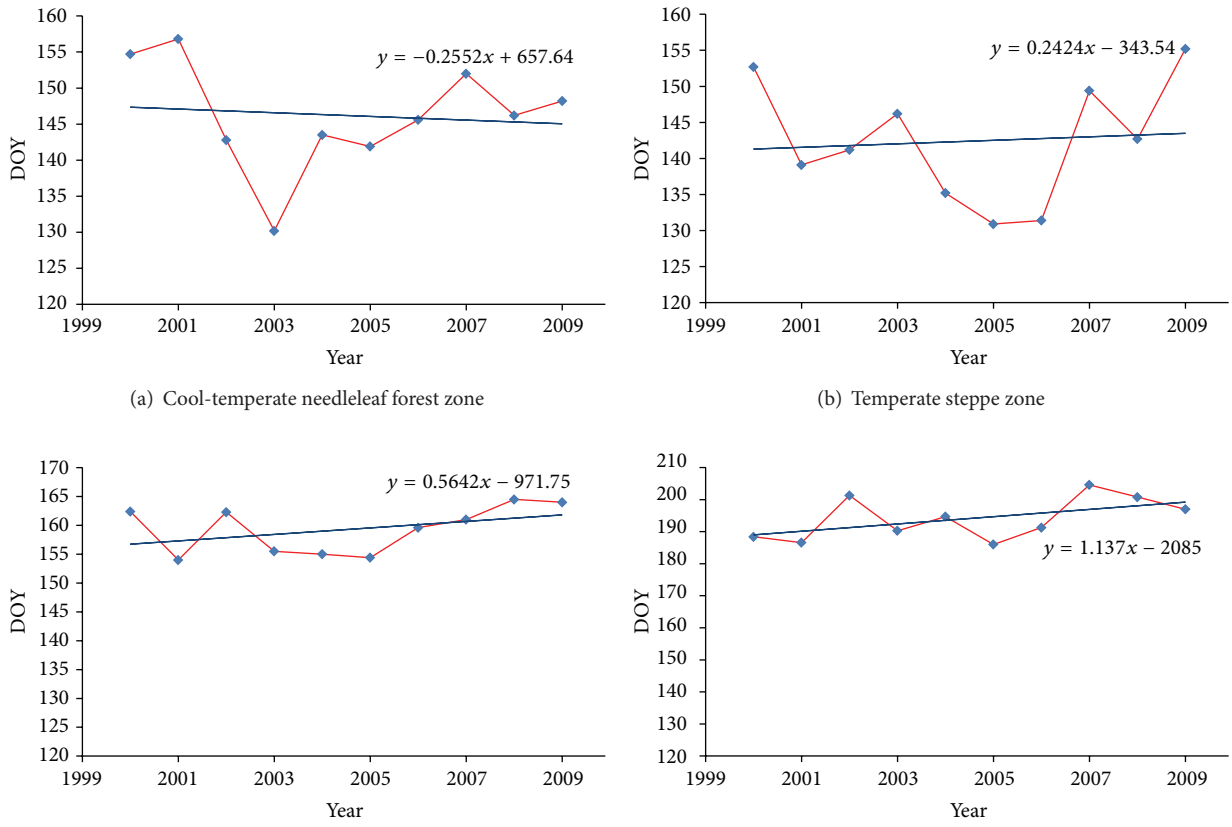

Figure 8: The average LOS trends in four vegetation zones.

Table 4: The correlation coefficients between climate and forest phenology (SOS) (2000–2009).

	SOS and temperature				SOS and precipitation			
	I	II	III	IV	I	II	III	IV
Annual average	0.44	−0.09	−0.29	0.00	−0.23	−0.33	0.66	−0.03
Spring	−0.30	−0.70*	−0.69*	−0.70*	0.00	0.37	0.43	−0.24
Winter	−0.03	−0.24	−0.35	−0.66	−0.11	0.37	0.00	0.30
February	0.00	−0.35	−0.28	−0.64	0.43	0.25	0.08	0.00
March	0.20	−0.22	−0.58*	−0.80**	0.13	−0.15	0.00	−0.55*
April	−0.45	−0.73**	−0.35	−0.27	0.09	0.27	−0.16	0.03
May	−0.72**	−0.55	−0.45	−0.33	0.37	0.34	0.44	0.45

Note. Trends are significant with $^{**}P < 0.01$, $^{*}P < 0.05$.
I: cool-temperate needleleaf forest region; II: temperate steppe region; III: temperate needleleaf and broadleaf mixed forest region; IV: warm-temperate deciduous broadleaf forest region.

To carry out the LOS correlation analysis, the mean meteorological variables (temperature and precipitation) of spring (from March to May), summer (from June to August), autumn (from September to November), and the entire year were used as the independent variables to calculate the correlation between climate and phenology (Table 6). The results showed that the LOS of the cool-temperate needleleaf forest region was positively correlated with the temperature of summer ($R = 0.50$, $P < 0.05$). In the temperate steppe region and temperate mixed-forest region, the LOS was positively correlated with the temperature of spring ($R = 0.58$, $P < 0.05$ and $R = 0.64$, $P < 0.05$, resp.). For these three regions, LOS was weakly correlated with the mean precipitation in all seasons. In the deciduous broadleaf forest region, the LOS had a positive correlation with the mean temperature of the year ($R = 0.74$, $P < 0.05$), yet it had a negative correlation

Table 5: The correlation coefficients between climate and forest phenology (EOS), 2000–2009.

	EOS and temperature				EOS and precipitation			
	I	II	III	IV	I	II	III	IV
Summer	0.38	0.47	0.18	0.09	0.00	−0.57	0.30	0.09
Autumn	0.71**	0.49	0.35	0.79**	−0.24	−0.56	−0.22	−0.45
July	0.14	0.32	0.00	−0.28	−0.08	−0.08	−0.32	0.28
August	0.58	0.73*	0.53	0.09	−0.08	−0.66*	0.36	−0.33
September	0.09	0.64*	0.00	0.29	−0.27	−0.53	−0.05	0.06
October	0.34	0.14	0.54*	0.70*	−0.14	0.00	−0.05	−0.48
November	0.68*	0.40	0.22	0.72*	−0.04	−0.57	−0.47	0.23

Note. Trends are significant with $^{**}P < 0.01$, $^{*}P < 0.05$.
I: cool-temperate needleleaf forest region; II: temperate steppe region; III: temperate needleleaf and broadleaf mixed forest region; IV: warm-temperate deciduous broadleaf forest region.

Table 6: The correlation coefficients between climate and forest phenology (LOS), 2000–2009.

	LOS and temperature				LOS and precipitation			
	I	II	III	IV	I	II	III	IV
Spring	−0.26	0.58*	0.64*	0.31	0.09	−0.34	0.00	0.35
Summer	0.50*	0.05	−0.16	−0.49	−0.24	0.11	−0.49	−0.16
Autumn	0.17	−0.46	−0.56	−0.22	−0.38	0.04	0.23	−0.40
Annual average	0.10	0.21	0.03	0.74*	−0.29	0.00	−0.19	−0.47*

Note. Trends are significant with $^{*}P < 0.05$.
I: cool-temperate needleleaf forest region; II: temperate steppe region; III: temperate needleleaf and broadleaf mixed forest region; IV: warm-temperate deciduous broadleaf forest region.

with the precipitation ($R = -0.47$, $P < 0.05$). Table 6 shows that LOS was positively correlated with temperature throughout the study area.

4. Conclusion and Discussion

In this study, we derived forest phenological variables (start of the growing season, end of the growing season, and length of the growing season) from the MODIS EVI time series data by the threshold-based method. In Northeast China, the average of SOS and EOS are 114 DOY and 278 DOY, respectively. Moreover, the forest phenological variables were found to be related to the distribution of forest types.

Based on the phenological variables extracted from EVI, we built spatial patterns of three forest phenological variables and the linear trends using the linear regression method. In Northeast China, the SOS was delayed, with the rates of 0~1.5 days per year. Although both advanced and delayed EOS were observed, the delay trend was more pervasive, with almost the same rates. As a result, the LOS increased slightly.

The analysis of the relationship between phenology and climate showed that the SOS (start of season) of each region was mainly affected by the spring temperature. Guo et al. came out with the same result using GIMMS NDVI time series between 1982 and 2003, which found that SOS of vegetation in Northeast China was significantly influenced by spring temperature [25]. Only the mean precipitation of March in the warm-temperate deciduous broadleaf forest region had a negative relationship with SOS ($R = -0.55$, $P < 0.05$). Except for the EOS (end of the growing season) of the temperate steppe region, which was affected by the temperature and precipitation of August, the EOS was significantly affected by temperature in the other study areas. The climate of different seasons had different influences in each area. Because of the increased temperature in spring, the LOS of the temperate steppe region and temperate mixed-forest region increased. The LOS of the cool-temperate needleleaf forest region was positively correlated with the temperature of summer ($R = 0.50$, $P < 0.05$), and the LOS of the deciduous broadleaf forest region was affected by both temperature and precipitation. Furthermore, the LOS was positively correlated with the mean temperature of the year ($R = 0.74$, $P < 0.05$) and negatively correlated with precipitation ($R = -0.47$, $P < 0.05$).

The average start of the growing season in the deciduous broadleaf forest region was advanced, but delayed in the needleleaf forest region, temperate steppe region, and temperate needleleaf and broadleaf mixed forest region. Due to the stronger delay in SOS compared to EOS, the LOS was decreased in the needleleaf forest region, a result that is not consistent with the result derived from the NDVI that needleleaf forest has advanced by rate of 2.5 days per year [39]. The discrepancy is most likely due to the different data and derivation method. The availability of methods and data specially developed for extracting phenological characteristics from remotely sensed data has simplified the data processing and made it more efficient. Vegetation phenology dynamics and its responses to meteorological variations can be described with such research. This study is helpful for phenology-linked climate change research and for

implementing climate-informed monitoring in the context of adaptive management [40].

Conflict of Interests

The authors declare that there is no conflict of interests regarding the publication of this paper.

Acknowledgments

This study was funded by the National Science Foundation of China (no. 41001279), Youth Science Funds of LREIS, CAS and Strategic Priority Research Program—Climate Change: Carbon Budget and Related Issues of the Chinese Academy of Sciences (nos. XDA05050102 and XDA05050602).

References

[1] A. D. Richardson, T. F. Keenan, M. Migliavacca, Y. Ryu, O. Sonnentag, and M. Toomey, "Climate change, phenology, and phenological control of vegetation feedbacks to the climate system," *Agricultural and Forest Meteorology*, vol. 169, pp. 156–173, 2013.

[2] X. Zhao, K. Tan, S. Zhao, and J. Fang, "Changing climate affects vegetation growth in the arid region of the northwestern China," *Journal of Arid Environments*, vol. 75, no. 10, pp. 946–952, 2011.

[3] Y. He, K. Lin, and X. Chen, "Effect of land use and climate change on runoff in the Dongjiang basin of south China," *Mathematical Problems in Engineering*, vol. 2013, Article ID 471429, 14 pages, 2013.

[4] C. O. Justice, J. R. G. Townshend, B. N. Holben, and C. J. Tucker, "Analysis of the phenology of global vegetation using meteorological satellite data," *International Journal of Remote Sensing*, vol. 6, no. 8, pp. 1271–1318, 1985.

[5] T. A. Stone, P. Schlesinger, R. A. Houghton, and G. M. Woodwell, "A map of the vegetation of South America based on satellite imagery," *Photogrammetric Engineering and Remote Sensing*, vol. 60, no. 5, pp. 541–551, 1994.

[6] J. Duncan, D. Stow, J. Franklin, and A. Hope, "Assessing the relationship between spectral vegetation indices and shrub cover in the Jornada Basin, New Mexico," *International Journal of Remote Sensing*, vol. 14, no. 18, pp. 3395–3416, 1993.

[7] M. A. White, P. E. Thornton, and S. W. Running, "A continental phenology model for monitoring vegetation responses to interannual climatic variability," *Global Biogeochemical Cycles*, vol. 11, no. 2, pp. 217–234, 1997.

[8] B. Duchemin, J. Goubier, and G. Courrier, "Monitoring phenological key stages and cycle duration of temperate deciduous forest ecosystems with NOAA/AVHRR data," *Remote Sensing of Environment*, vol. 67, no. 1, pp. 68–82, 1999.

[9] X. Zhang, M. A. Friedl, C. B. Schaaf et al., "Monitoring vegetation phenology using MODIS," *Remote Sensing of Environment*, vol. 84, no. 3, pp. 471–475, 2003.

[10] X. Zhang and M. D. Goldberg, "Monitoring fall foliage coloration dynamics using time-series satellite data," *Remote Sensing of Environment*, vol. 115, no. 2, pp. 382–391, 2011.

[11] K. Soudani, G. le Maire, E. Dufrêne et al., "Evaluation of the onset of green-up in temperate deciduous broadleaf forests derived from Moderate Resolution Imaging Spectroradiometer (MODIS) data," *Remote Sensing of Environment*, vol. 112, no. 5, pp. 2643–2655, 2008.

[12] P. Lesica and P. M. Kittelson, "Precipitation and temperature are associated with advanced flowering phenology in a semi-arid grassland," *Journal of Arid Environments*, vol. 74, no. 9, pp. 1013–1017, 2010.

[13] R. Herdianto, K. Paik, N. A. Coles, and K. Smettem, "Transitional responses of vegetation activities to temperature variations: insights obtained from a forested catchment in Korea," *Journal of Hydrology*, vol. 484, pp. 86–95, 2013.

[14] J. Kariyeva and W. J. D. van Leeuwen, "Environmental drivers of NDVI-based vegetation phenology in Central Asia," *Remote Sensing*, vol. 3, no. 2, pp. 203–246, 2011.

[15] D. Pouliot, R. Latifovic, R. Fernandes, and I. Olthof, "Evaluation of compositing period and AVHRR and MERIS combination for improvement of spring phenology detection in deciduous forests," *Remote Sensing of Environment*, vol. 115, no. 1, pp. 158–166, 2011.

[16] E. G. Beaubien and H. J. Freeland, "Spring phenology trends in Alberta, Canada: links to ocean temperature," *International Journal of Biometeorology*, vol. 44, no. 2, pp. 53–59, 2000.

[17] R. de Jong, S. de Bruin, A. de Wit, M. E. Schaepman, and D. L. Dent, "Analysis of monotonic greening and browning trends from global NDVI time-series," *Remote Sensing of Environment*, vol. 115, no. 2, pp. 692–702, 2011.

[18] S. Potithep, S. Nagai, K. N. Nasahara, H. Muraoka, and R. Suzuki, "Two separate periods of the LAI-VIs relationships using in situ measurements in a deciduous broadleaf forest," *Agricultural and Forest Meteorology*, vol. 169, pp. 148–155, 2013.

[19] X. Q. Chen, Z. J. Tan, M. D. Schwartz, and C. Xu, "Determining the growing season of land vegetation on the basis of plant phenology and satellite data in Northern China," *International Journal of Biometeorology*, vol. 44, no. 2, pp. 97–101, 2000.

[20] X. Q. Chen, C. X. Xu, and Z. J. Tan, "An analysis of relationships among plant community phenology and seasonal metrics of normalized difference vegetation index in the northern part of the monsoon region of China," *International Journal of Biometeorology*, vol. 45, no. 4, pp. 170–177, 2001.

[21] X. Q. Chen and W. F. Pan, "Relationships among phenological growing season, time-integrated normalized difference vegetation index and climate forcing in the temperature region of Eastern China," *International Journal of Climatology*, vol. 22, no. 14, pp. 1781–1792, 2002.

[22] X. Chen, L. Vierling, D. Deering, and A. Conley, "Monitoring boreal forest leaf area index across a Siberian burn chronosequence: a MODIS validation study," *International Journal of Remote Sensing*, vol. 26, no. 24, pp. 5433–5451, 2005.

[23] X. Chen and L. Xu, "Temperature controls on the spatial pattern of tree phenology in China's temperate zone," *Agricultural and Forest Meteorology*, vol. 154-155, pp. 195–202, 2012.

[24] G. Zhang, Y. Zhang, J. Dong, and X. Xiao, "Green-up dates in the Tibetan Plateau have continuously advanced from 1982 to 2011," *Proceedings of the National Academy of Sciences of the United States of America*, vol. 110, no. 11, pp. 4309–4314, 2013.

[25] Z. Guo, X. Zhang, Z. Wang, and W. Fang, "Responses of vegetation phenology in Northeast China to climate change," *Chinese Journal of Ecology*, vol. 29, no. 3, pp. 578–585, 2010 (Chinese).

[26] D. Mao, Z. Wang, L. Luo, and C. Ren, "Integrating AVHRR and MODIS data to monitor NDVI changes and their: relationships with climatic parameters in Northeast China," *International Journal of Applied Earth Observation and Geoinformation*, vol. 18, no. 1, pp. 528–536, 2012.

[27] Y. Ye and X. Fang, "Land use change in Northeast China in the twentieth century: a note on sources, methods and patterns," *Journal of Historical Geography*, vol. 35, no. 2, pp. 311–329, 2009.

[28] A. R. Huete, H. Q. Liu, K. Batchily, and W. van Leeuwen, "A comparison of vegetation indices over a global set of TM images for EOS-MODIS," *Remote Sensing of Environment*, vol. 59, no. 3, pp. 440–451, 1997.

[29] A. Huete, K. Didan, T. Miura, E. P. Rodriguez, X. Gao, and L. G. Ferreira, "Overview of the radiometric and biophysical performance of the MODIS vegetation indices," *Remote Sensing of Environment*, vol. 83, no. 1-2, pp. 195–213, 2002.

[30] J. Liu, W. Kuang, Z. Zhang et al., "Spatiotemporal characteristics, patterns, and causes of land-use changes in China since the late 1980s," *Journal of Geographical Sciences*, vol. 24, no. 2, pp. 195–210, 2014.

[31] P. S. A. Beck, C. Atzberger, K. A. Høgda, B. Johansen, and A. K. Skidmore, "Improved monitoring of vegetation dynamics at very high latitudes: a new method using MODIS NDVI," *Remote Sensing of Environment*, vol. 100, no. 3, pp. 321–334, 2006.

[32] P. M. Atkinson, C. Jeganathan, J. Dash, and C. Atzberger, "Inter-comparison of four models for smoothing satellite sensor time-series data to estimate vegetation phenology," *Remote Sensing of Environment*, vol. 123, pp. 400–417, 2012.

[33] P. Jönsson and L. Eklundh, "TIMESAT—a program for analyzing time-series of satellite sensor data," *Computers and Geosciences*, vol. 30, no. 8, pp. 833–845, 2004.

[34] J. N. Hird and G. J. McDermid, "Noise reduction of NDVI time series: an empirical comparison of selected techniques," *Remote Sensing of Environment*, vol. 113, no. 1, pp. 248–258, 2009.

[35] X. Yu, D. Zhuang, X. Hou, and H. Chen, "Forest phenological patterns of Northeast China inferred from MODIS data," *Journal of Geographical Sciences*, vol. 15, no. 2, pp. 239–246, 2005.

[36] X. Yu, D. Zhuang, H. Chen, and X. Hou, "Forest classification based on MODIS time series and vegetation phenology," in *Proceedings of the IEEE International on Geoscience and Remote Sensing Symposium (IGARSS '04)*, vol. 4, pp. 2369–2372, September 2004.

[37] U. B. Shrestha, S. Gautam, and K. S. Bawa, "Widespread climate change in the Himalayas and associated changes in local ecosystems," *PLoS ONE*, vol. 7, no. 5, Article ID e36741, 2012.

[38] G. Ma, L. Dong, and X. Wang, "Study on the dynamically monitoring and simulating the vegetation cover in Northwest China in the past 21 years," *Journal of Glaciology and Geocryology*, vol. 25, no. 2, pp. 1000–0240, 2003 (Chinese).

[39] Z. Guo, X. Zhang, Z. Wang, and W. Fang, "Simulation and variation pattern of vegetation phenology in Northeast China based on remote sensing," *Chinese Journal of Ecology*, vol. 29, no. 1, pp. 165–172, 2010 (Chinese).

[40] C. A. F. Enquist, J. L. Kellermann, K. L. Gerst, and A. J. Miller-Rushing, "Phenology research for natural resource management in the United States," *International Journal of Biometeorology*, vol. 58, no. 4, pp. 579–589, 2014.